POLITECNICO DI TORINO
Repository ISTITUZIONALE

Vehicle4em: An Open Database of Vehicle CAD Models for Electromagnetic Simulations

Original
Vehicle4em: An Open Database of Vehicle CAD Models for Electromagnetic Simulations / Freschi, F., Giaccone, L., Cirimele, V., Solimene, L.. - In: IEEE JOURNAL ON WIRELESS POWER TECHNOLOGIES. - ISSN 3066-5736. - ELETTRONICO. - 1:(2026), pp. 1-10. [10.1109/jwpt.2026.3672392]

Availability:
This version is available at: 11583/3016928 since: 2026-10-24T08:27:36Z

Publisher:
Institute of Electrical and Electronics Engineers

Published
DOI:10.1109/jwpt.2026.3672392

Terms of use:

This article is made available under terms and conditions as specified in the corresponding bibliographic description in the repository

Publisher copyright

(Article begins on next page)

16 November 2026

Vehicle4em: An Open Database of Vehicle CAD Models for Electromagnetic Simulations

Fabio Freschi, *Senior Member, IEEE*, Luca Giaccone, *Senior Member, IEEE*, Vincenzo Cirimele, *Senior Member, IEEE*, and Luigi Solimene, *Member, IEEE*

***Abstract*—This study introduces CAD-based vehicle models optimized for electromagnetic simulations, with a focus on wireless power transfer (WPT) assessment. The models balance geometric detail and computational efficiency to enable accurate analysis of electromagnetic interactions and human exposure. Mesh quality assessments and the reported numerical evaluations confirm their suitability for compliance-oriented studies. The Fiat 500 model is used in a case study to demonstrate applicability to ICNIRP guideline assessments. The database is freely available under the MIT license on GitHub and includes STEP CAD files and volumetric meshes, providing a practical resource for research on WPT-related EMC and exposure in automotive applications.**

***Index Terms*—CAD models, dynamic charging systems, numerical dosimetry, wireless power transfer.**

I. Introduction

AFTER many years of extensive research, resonant inductive charging technology, often more generically referred to as wireless power transfer (WPT), has reached a stage of technological maturity [1], [2]. This is especially true for static applications, i.e., with the vehicle parked during the charging process, for which there are already both automotive and electric standards, such as SAE J2954 [3], [4], [5] and IEC 61980 [6], [7]. These advancements have sparked interest from car manufacturers, many of whom are evaluating the incorporation of WPT systems into their electric models [1].

In addition to static applications, the interest of the technical and scientific community remains high with respect to the extension of this technology towards its application with moving vehicles, commonly referred to as dynamic WPT [2], [8], [9].

Received 2 November 2025; revised 28 January 2026; accepted 6 March 2026. Date of publication 11 March 2026; date of current version 27 March 2026. This work was supported by the Italian Ministry of University and Research (MUR) under the Call for tender No. 104 published on 2.2.2022. Project Title "Electromagnetic modeling and design of WPT systems in compliance with EMC and safety guidelines for automotive applications" - CUP E53C24002470006. The associate editor coordinating the review of this article and approving it for publication was Dr. Alessandra Costanzo. *(Corresponding author: Luca Giaccone.)*

Fabio Freschi, Luca Giaccone, and Luigi Solimene are with the Dipartimento Energia "G. Ferraris", Politecnico di Torino, 10129 Torino, Italy (e-mail: fabio.freschi@polito.it; luca.giaccone@polito.it; luigi.solimene@polito.it).

Vincenzo Cirimele is with the Department of Electrical, Electronic, and Information Engineering "G. Marconi", University of Bologna, 40136 Bologna, Italy (e-mail: vincenzo.cirimele@unibo.it).

Digital Object Identifier 10.1109/JWPT.2026.3672392

As evidenced by several scientific studies [4], [10], [11] and the evolution of the standards themselves, the development and pre-commercialization of such charging systems is accompanied by the development of increasingly accurate methodologies for assessing user exposure to the magnetic fields. Exposure is indeed one of the main issues with WPT systems, as the typical distance between the transmitter and receiver coils, which is in the order of tens of centimeters, gives rise to a stray field near the vehicle chassis. These aspects are naturally crucial for the safety and social acceptance of this technology.

The aforementioned standards all agree on a nominal operating frequency for these systems of 85 kHz. At this frequency, electromagnetic phenomena occurring near the surface of all conductive elements in the vicinity of the coils become relevant. In this context, all problems related to the computation of the electromagnetic field distribution generated by a WPT system, such as those aimed at the analysis of electromagnetic compatibility (EMC) or human exposure, require the evaluation of the interaction with the car body, which is characterized by the presence of ferromagnetic and conductive materials and therefore affected by the development of eddy currents in extremely small thicknesses (typically less than one millimeter).

To address these issues, detailed electromagnetic simulations are essential. Such simulations must account for the complex geometries of car bodies, which are designed to meet mechanical, aesthetic, and aerodynamic requirements. The geometry of a car body often includes intricate structures and a variety of materials, such as ferromagnetic components, conductive sheets, and non-conductive elements, all of which must be considered in the modeling process.

This problem has been approached in different ways so far. Some works greatly simplify the geometries with stylised shapes [12], [13], [14] or by representing the entire car body by means of simple planes of conductive material [15], [16]. Other works consider only some parts of the vehicle, mainly the floor, which is the part most directly exposed to the fields generated by the coils [17], [18]. Although this approach allows for reproducing with good approximation the field distribution at the WPT system level, it may not allow a reliable evaluation of the overall distribution in the upper part of the vehicle and, in particular, that in the passenger compartment volume.

Some more recent works use chassis models provided by car manufacturers, often by not considering some parts as axles, joints, or wheels [17], [19]. These models are typically derived from graphical design files regarding the exterior part of the vehicle. Although such models are typically more descriptive of

© 2026 The Authors. This work is licensed under a Creative Commons Attribution 4.0 License. For more information, see https://creativecommons.org/licenses/by/4.0/

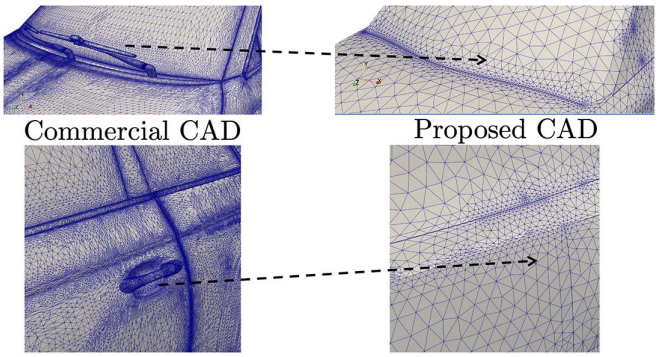


Fig. 1. Commercial CADs (left) typically contain mechanical details that are unnecessary for electromagnetic simulations. The proposed models (right) simplify such details (e.g., windshield wipers and door handles) to improve mesh generation.

the actual shape of the vehicle, to be used effectively, they still require various corrective actions to ensure the consistency of the model. In particular, in electromagnetic analysis, it is of extreme importance to have a correct correspondence between volume regions of conductive or ferromagnetic materials and their surfaces. These regions are usually connected by welding, allowing the car body to become a whole conducting region. Unfortunately, these conditions are not always met by the graphical files, which define lines and surfaces on the basis of geometric tolerances that are sometimes not congruent with the continuity of electrical domains. As a consequence, the electromagnetic model has to be checked carefully and locally and manually corrected to enforce the continuity of conductive parts.

Once an electromagnetic model is obtained, the next challenge lies in its discretization for numerical simulations involving the coil assemblies. This process requires careful meshing of both the surface and the volume of the conductive parts. Ensuring a good mesh quality is critical to achieving a reliable and robust field solution. However, this task is inherently complex due to the several orders of magnitude in scale between the car's overall dimensions and the thickness of its metal sheets.

To address these challenges, this work presents a series of CAD-based car and light commercial vehicle models specifically designed for electromagnetic simulations. Ad hoc CAD models are needed because commercial CAD assemblies typically contain mechanical details that are unnecessary for electromagnetic simulations and can hinder the generation of high-quality meshes. For this reason, models are proposed that strike a balance between geometric detail and computational efficiency, enabling accurate analysis of WPT systems while maintaining manageable simulation times. Examples of simplifications include the removal of windshield wipers and door handles as shown in Fig. 1.

The CAD models are structured to allow flexibility in their use, with modular components that can be selectively included or excluded depending on the simulation requirements. This work, which is an extension of the conference proceeding [20], presents the process followed for the realization of these models and the techniques applied to bring the overall quality of the entire models' mesh to a good compromise for electromagnetic

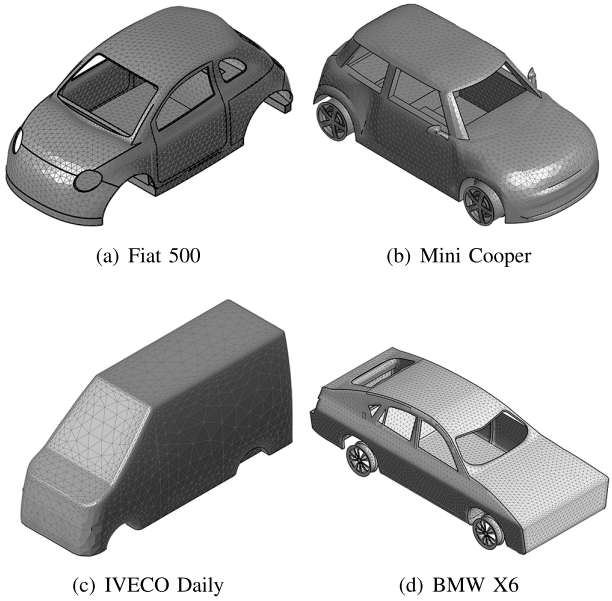


Fig. 2. Four vehicle models: Fiat 500 (a), mini cooper (b), IVECO daily (c), and BMW X6 (d).

computations. The effectiveness of the models and their discretization is presented and discussed through the solution of an electromagnetic problem involving the car models and a WPT structure compliant with the SAE J2954 standard. A complete case study is also provided, considering the application to numerical dosimetry.

Following an extensive validation phase, including scientific studies based on the proposed models [21], [22], the Vehicle4em database is made publicly available via the repository in [23] under the MIT license. It provides four vehicle models in STEP format, together with basic scripts and instructions to download and visualize the data.

II. Vehicle4em Database

The database comprises the four vehicle models shown in Fig. 2: Fiat 500, Mini Cooper, IVECO Daily, and BMW X6. All models are available in a GitHub repository [23]. At the time of writing, the models are provided in `STEP` format, a standardized format used for exchanging 3D models between different CAD software. These files can be used to obtain a mesh with whichever software best suits the user's needs. Moreover, each model is also provided with a volumetric unstructured mesh stored in a `.vtu` file.

A. Properties of the Models

To optimize the CAD models for electromagnetic simulations, simplifications were introduced to prioritize computational efficiency over detailed geometric representation. Small components, such as gears, transmission parts, and screws, were excluded due to their negligible impact on electromagnetic field simulations. Similarly, non-metallic components, including steering wheels, seats, and other plastic parts, were omitted to reduce complexity. Larger elements, such as windscreens, tires,

TABLE I
NUMBER OF ELEMENTS AND MEDIAN VALUE OF THE MESH QUALITY INDEX FOR THE 3D AND 2D MESHES AVAILABLE IN THE DATABASE

Model	No. tetrahedra	$\tilde{q}_{3D}$	No. Triangles	$\tilde{q}_{2D}$
Fiat 500	56,219	0.675	129,041	0.904
BMW X6	135,631	0.437	302,844	0.719
Mini Cooper	42,111	0.687	93,529	0.858
Iveco Daily	248,875	0.23	558,675	0.825

and windows, have been included. For the low-frequency analyses considered here, these dielectric parts can be neglected with limited impact on the solution. They may become relevant at higher frequencies, where dielectric interactions contribute more significantly to field distributions.

Additional geometric simplifications were applied to reduce the computational cost of meshing. Complex geometries were replaced with smooth, linear surfaces, favoring simple rectangular or circular shapes with minimal fillets and chamfers. The resulting parts are represented as three-dimensional non-intersecting solids, ensuring a watertight model free of holes or non-manifold edges. The models are modular, allowing doors and hatches to be opened or closed to evaluate their impact on electromagnetic field patterns.

To allow for the greatest flexibility, the material properties of the different parts are not hard-coded but can be set by the user according to the specific problem being studied. This broadens the applicability of the shared CAD models to electromagnetic problems other than the WPT case addressed here. As an example, since the CAD models are already available to the scientific community, an independent work uses one of the proposed CAD for the optimal design of an antenna operating in the sub-6 GHz band [24].

The generated CAD models closely approximate real vehicles while maintaining suitability for electromagnetic analysis. Geometrical optimizations streamlined the modeling process, with dimensions obtained through a combination of direct measurements and analysis of photographs or renderings using specialized software. Minor dimensional inaccuracies were deemed acceptable given the study's objectives. SolidWorks (Dassault Systèmes) was used to construct the models, which are organized using modular trees and sub-trees to enable easy inclusion or exclusion of specific components.

B. Accessing and Visualizing the Models

The volumetric meshes are provided in the VTK XML unstructured-grid format `.vtu`. The `.vtu` format is an XML-based representation of unstructured grid datasets employed by the Visualization ToolKit (VTK) [25], [26]. The `.vtu` files can be directly opened in ParaView [27] for inspection and visualization. For completeness, the main statistics of the volumetric meshes provided with Vehicle4em are reported in Table I. The table lists the number of nodes and tetrahedra of each model, the number of surface triangles together with the median value of the mesh quality index (see Sec. IV for details) computed on the distributed meshes. These values refer to the meshes included in the repository and may differ if the geometry is remeshed with different settings.

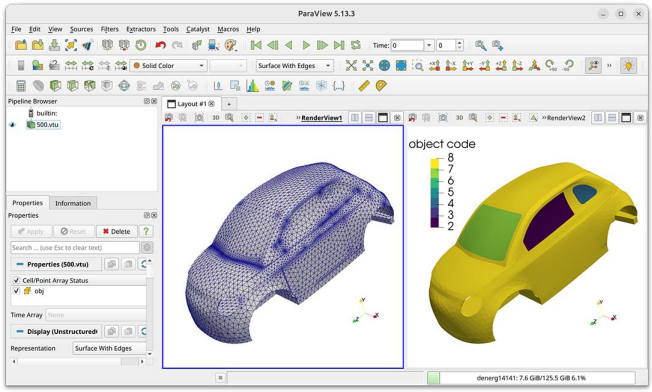


Fig. 3. ParaView - An open-source and multiple-platform application for interactive, scientific visualization.

As shown in Fig. 3, one simply needs to drag and drop the `.vtu` file into the Pipeline Browser and click the *Apply* button to display the model. ParaView further enables users to manipulate and render the model, as illustrated in Fig. 3. Since ParaView is thoroughly documented, providing additional details is beyond the scope of this paper.

To further reduce barriers to accessing the models, a short Python script is provided for loading the `.vtu` files. The script, named `import_mesh.py`, is based on the Python module `meshio` [28]. As shown at the end of this subsection, the script is largely self-explanatory: (i) the `.vtu` file is loaded into memory, and (ii) the points, connectivity, and object codes are extracted and stored in dedicated variables. From that point onward, the user can manipulate these variables as needed.

```
import meshio

# import mesh
mesh = meshio.read("500.vtu")

# get points
points = mesh.points

# get connectivity
connectivity = mesh.cells[0].data

# get object codes
obj = mesh.cell_data["obj"][0]
```

III. WHY DETAILED VEHICLE MODELS MATTER FOR ELECTROMAGNETIC SIMULATION

In automotive WPT scenarios, the vehicle body strongly influences the electromagnetic solution because it supports the dominant induced-current paths. As a result, both geometric simplifications and differences among vehicle geometries can modify current flow and change the magnetic-field distribution in regions relevant to occupants. The following analyses quantify these effects under identical excitation and evaluation settings.

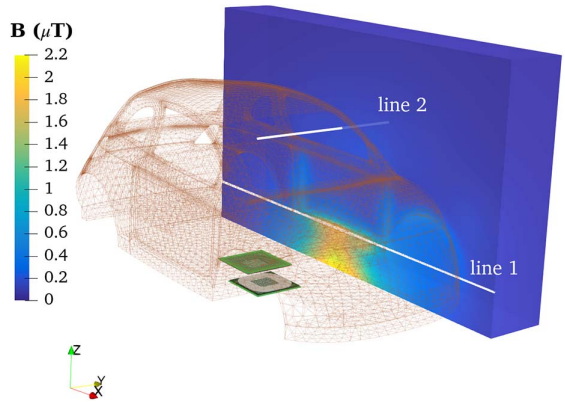


Fig. 4. Magnetic field generated by the WPT system considering the Fiat 500 CAD model. The field is computed on an inspection volume at the side of the vehicle and also along two inspection lines called *line 1* and *line 2*.

A. Effect of the Chassis Approximation

The first analysis regards the influence of different levels of the chassis approximation on the magnetic stray field in the region adjacent to the vehicle. The source of magnetic field is a WPT system as shown in Fig. 4. It is classified as WPT2/Z3 according to the SAE J2954 standard [3], the transmitter is centered with respect to the car body, while the receiver is laterally offset in the y-direction by 100 mm, which corresponds to the maximum misalignment permitted by the SAE J2954 standard [3]. The vertical distance between the receiver and the car body floor is 30 mm. The clearance between the receiver coil and the ground is 196.8 mm. The input power is set to 7.7 kW, which corresponds to the complex coil currents 26 A (transmitter) and j26 A (receiver) for the adopted operating conditions. The operating frequency is fixed at 85 kHz. Each coil consists of 8 turns and is shielded by two thin layers, one of aluminum and one of ferrite, with outer dimensions of 420 mm $\times$ 420 mm. It is important to stress that the layout described is intended solely as a supporting example and does not aim to draw general conclusions about the safety of the considered specific vehicles and mounting positions. For brevity, this section considers only the Fiat 500 CAD model because the aim is to consider a full vehicle geometry with extremely simplified chassis.

With reference to Fig. 4, the stray magnetic flux density is evaluated over the lateral inspection volume that spans the full vehicle length along the x direction (3555 mm). Along y, the volume starts at an air gap of approximately 2 mm from the outer surface of the chassis and extends outward for 500 mm. The base of the volume lies on the xy plane at $z = 0$, and its height is 2000 mm. As illustrated in Fig. 4, the stray field is maximum in the lower and central portion of the inspection volume, i.e., in the region closest to the WPT system and least shielded by the chassis. The peak value reaches 2.2 μT. In addition, field points close to the vehicle surface exhibit localized variations due to eddy currents induced in the conductive chassis: in the vicinity of the chassis (within the xz plane shown), the field typically falls in the range 0.7–1.0 μT. These near-body features are geometry-dependent and are therefore expected to be altered when the chassis is replaced by simplified representations.

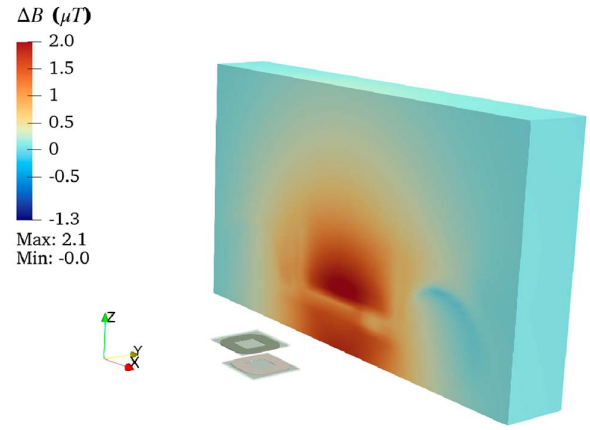
Finally, Fig. 4 also reports two inspection lines used for a quantitative comparison of the stray magnetic field. *Line 1* is oriented along the x direction and lies in the xz plane, close to the vehicle side, at a height of $z = 350$ mm. *Line 2* is oriented along the y direction and is defined so as to cross the vehicle boundary: it starts from a point inside the vehicle and extends outward, terminating at a point on the outer xz plane of the inspection volume (i.e., the plane farthest from the vehicle along x). The same computations are repeated for three cases: (a) the WPT system in free space (no vehicle/chassis), (b) the floor panel extracted from the full vehicle CAD, modeled with a uniform thickness of 10 mm, used here as an envelope thickness capturing the overall depth introduced by curvatures, folds, and local reinforcements, and (c) an equivalent rectangular prism (bounding box) that encloses the floor geometry and matches its outer dimensions, adopting the same envelope thickness (10 mm). For each case, the absolute deviation of the magnetic flux density magnitude is computed as $\Delta B = B - B_{\text{ref}}$, where B is the magnetic flux density magnitude for the case under consideration (a–c) and B_{ref} is the corresponding magnitude for the full-vehicle reference case shown in Fig. 4. The resulting ΔB maps (in μT) are shown in Fig. 5(a)–5(c).

The no-chassis case yields the largest positive deviations, indicating a systematic overestimation of the stray field; locally, the predicted field magnitude reaches approximately twice the reference values. The largest negative deviations occur for the equivalent rectangular floor, which underestimates the field compared to the full-geometry model (down to about $1/1.3$ of the reference in the most affected regions). To facilitate visual comparison, all maps are displayed using the same saturation limits; the actual minimum and maximum ΔB values for each case are reported below each colorbar.

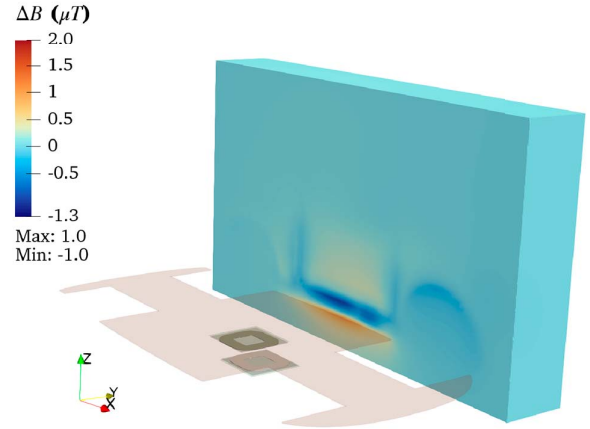
A more quantitative comparison is provided by evaluating the magnetic flux density along the two inspection lines introduced above. The results along *line 1* are reported in Fig. 6. The full-vehicle reference solution (blue curve) is not symmetric because the field distribution is influenced by the proximity with the chassis, which is not symmetric. Both simplified-chassis models underestimate the stray field along the entire line, whereas the no-chassis case yields a systematic overestimation over the full line extent.

Fig. 7 completes the comparison because inspection *line 2* partially lies inside the vehicle (approximately for $y < 0.7$ m). For the full-vehicle reference case, a clear change in slope is observed around $y \approx 0.7$ m, corresponding to the intersection of the line with the side-window region of the vehicle. In particular, the field exhibits a local maximum near the side-window region and decreases on both sides of this location. This feature is not reproduced by the simplified chassis models and, as expected, it is absent in the no-chassis case. Along *line 2*, both the no-chassis and the floor-only cases systematically overestimate the field. The equivalent rectangular prism overestimates the field for $y < 0.4$ m, while it underestimates the field over the remaining portion of the line.

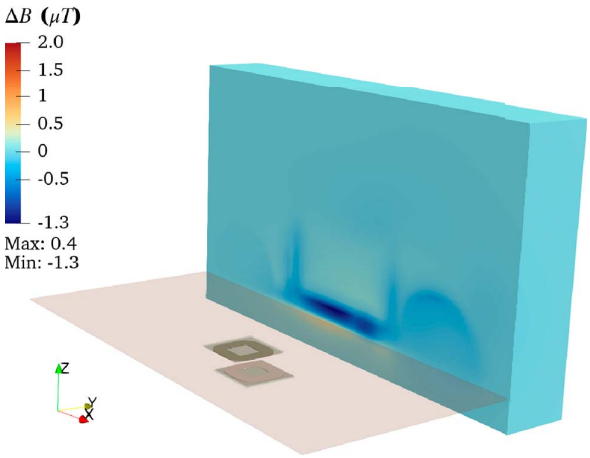
Overall, these results validate the need to employ the full vehicle CAD geometry to obtain reliable stray-field predictions, since simplified chassis representations can introduce



(a)



(b)



(c)

Fig. 5. Deviation of the magnetic flux density from the reference case. WPT system in free space, no vehicle/chassis (a), floor panel extracted from the full vehicle CAD (b) and equivalent rectangular prism (bounding box) that encloses the floor geometry (c).

substantial, spatially dependent over- and underestimations of the magnetic flux density; in particular, because conductive shielding is affected by edge effects (increased eddy-current density near boundaries [29]), simplified models may introduce artificial edges that are not present in the real chassis, leading to localized errors near those boundaries.

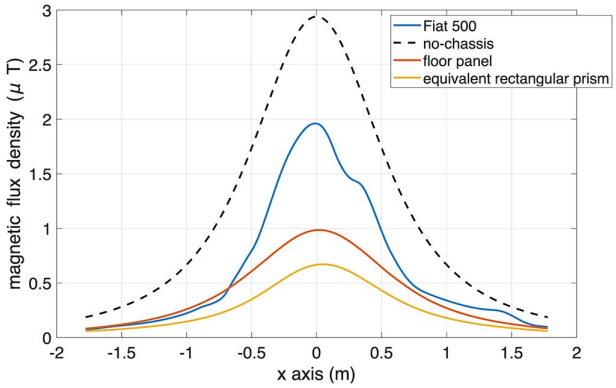


Fig. 6. Magnetic flux density along *line 1* for the reference case, the no-chassis case and the simplified chassis cases.

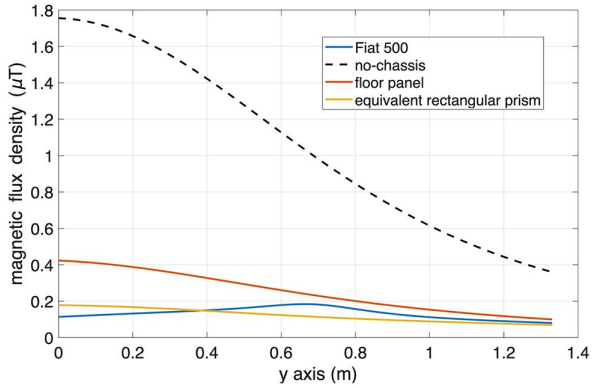


Fig. 7. Magnetic flux density along *line 2* for the reference case, the no-chassis case and the simplified chassis cases.

B. Impact of Geometric Variability Across Vehicles on Electromagnetic Simulation

In this section, the influence of the CAD model on the stray field generated by a WPT system is analyzed. The WPT system under consideration is the same as in Sec. III-A. The magnetic flux density is computed on the inspection plane shown in Fig. 8(a) and 8(b). Differently from Sec. III-A, this plane is not defined with absolute coordinates. As shown in Fig. 8(a) it is defined with respect to the dimensions of the vehicle considered. The inspection plane lies in the x-z plane, located 200 mm away from the car body, and spans an area of 4 m $\times$ 2 m in the x and z directions, respectively. The magnetic flux density is computed for all the CAD models and the results are presented in Fig. 9(a)–9(d). All plots are saturated using the same range, ($B_{\min} = 0$ μT $- B_{\max} = 1.8$ μT). It is evident that the car body geometry significantly affects the stray magnetic field. The Fiat 500 and the IVECO Daily exhibit the strongest shielding effect, while the Mini Cooper and BMW X6 show comparable maximum field values but differ in terms of spatial distribution.

To enable a more quantitative comparison, two inspection lines are defined, as shown in Fig. 8(b). The first line corresponds to the bottom edge of the inspection plane and is

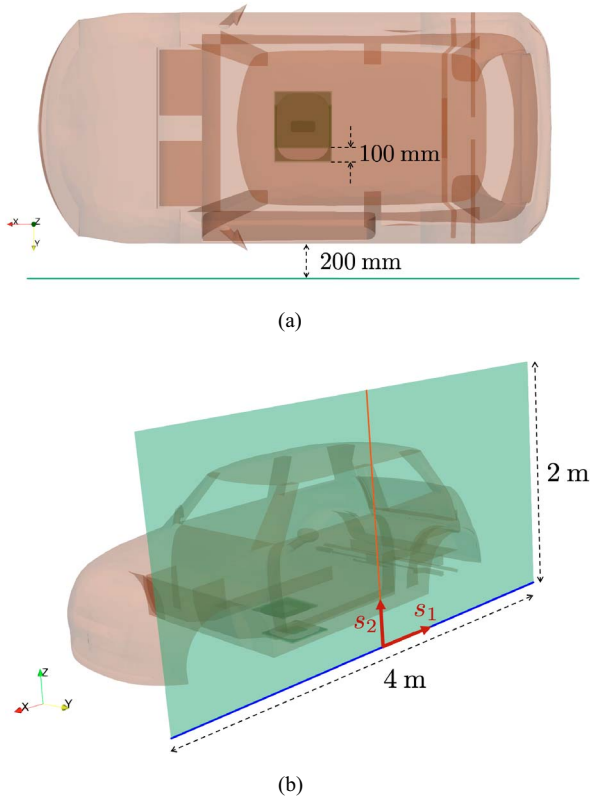


Fig. 8. Dimensions and position of the inspection plane and the two inspection lines.

depicted in blue. The second line is orthogonal to the first and is positioned at the center of the inspection plane. A local coordinate system, (s_1, s_2), is introduced to plot the magnetic flux density values along these lines. The results are shown in Fig. 10. The same observations discussed for Fig. 9 remain valid. From these plots, it becomes clearer that the maximum magnetic flux density for the Mini Cooper and the BMW X6 is approximately twice the value observed for the Fiat 500 and the IVECO Daily.

IV. End-to-End Workflow Case Study

This section shows a complete case study where the Fiat 500 CAD model is used to study the exposure of a person standing next to the car during the wireless charging phase.

Starting from the STEP file available in the database, a 3D tetrahedral mesh is generated. During preprocessing, intersecting or self-intersecting components were removed through minor CAD-level edits (e.g., small local offsets or tolerance adjustments) applied only to restore geometric consistency. After these corrections, the model can be discretized and used in electromagnetic simulations without additional manual intervention. The geometrical objects used to reconstruct the vehicle geometry are intrinsically multi-scale, with the vehicle dimensions in the order of meters and the thickness of the metal sheets in the order of millimeters.

Assuming electrical properties of common steel for automotive applications [30], e.g. $\sigma = 2 \times 10^6$ S/m and $\mu_r = 300$, which correspond to a common type of steel with moderate shielding capabilities [21], [22], [30], the skin depth is about

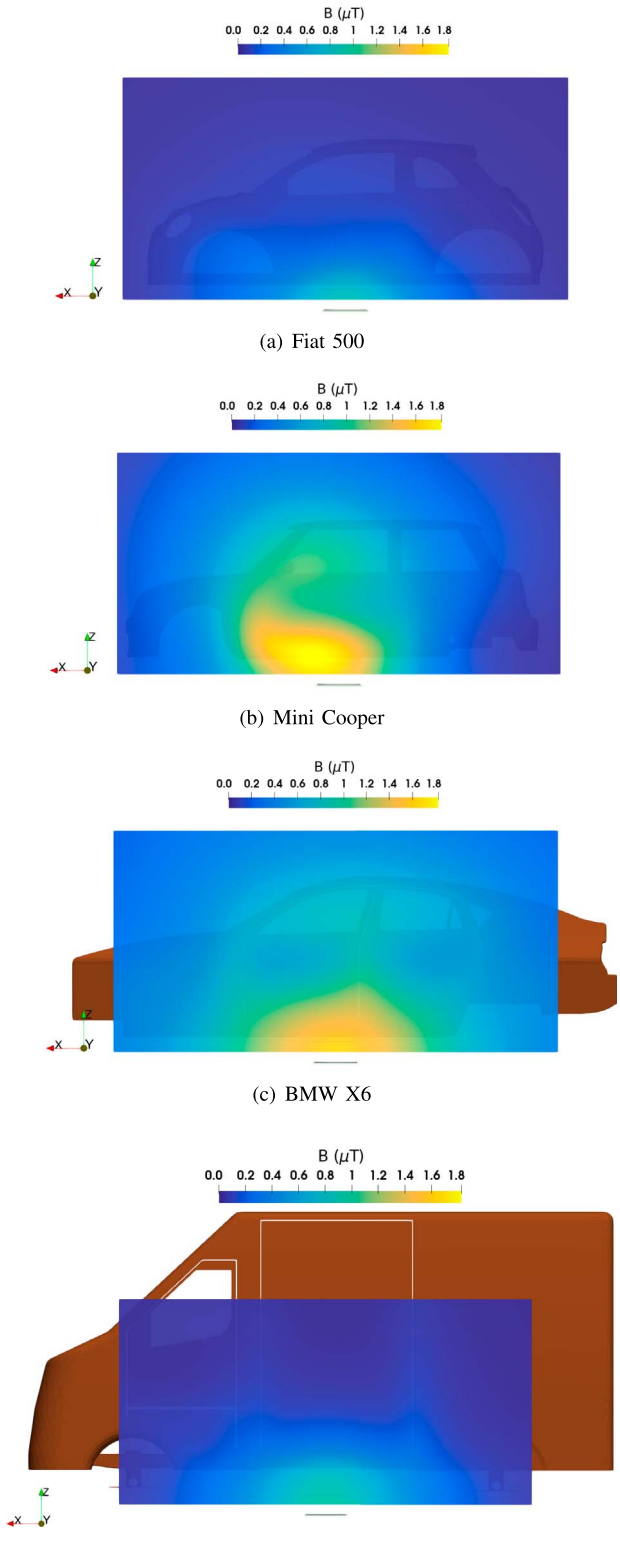


Fig. 9. Magnetic flux density on the inspection plane for different CAD models. Fiat 500 (a), mini cooper (b), and BMW X6 (c) and IVECO daily (d).

70 μm, further amplifying the large aspect ratio issue. Achieving regular tetrahedra while explicitly resolving the eddy-current distribution would require element sizes on the order of the skin depth, which is far smaller than the characteristic geometric dimensions of the chassis and leads to prohibitively large

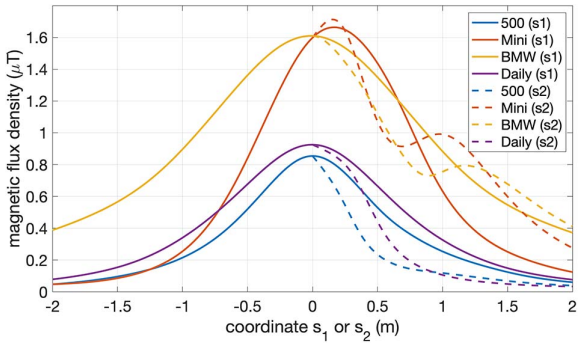


Fig. 10. Magnetic flux density along the two inspection lines.

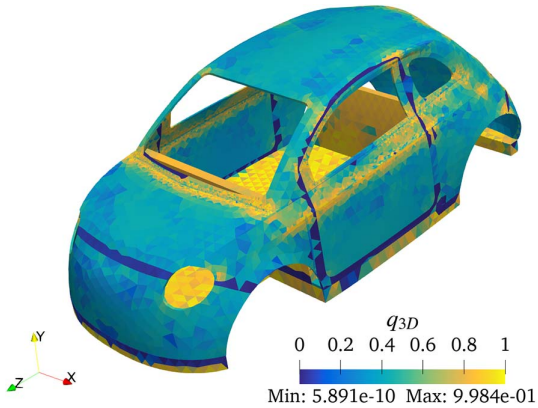


Fig. 11. Map of the 3D mesh quality for the Fiat 500 model.

meshes. Conversely, allowing large elements in regions such as the roof, bonnet, or doors typically produces high-aspect-ratio tetrahedra, which degrades numerical robustness. This trade-off motivates assessing mesh quality explicitly and, when needed, adopting surface-based formulations. The quality of the volumetric mesh can be assessed by computing the quality index defined as the ratio between the radius $r_{in,3D}$ of the inscribed sphere and the radius $r_{circ,3D}$ of the circumscribed sphere for each tetrahedron:

$$q_{3D} = 3\frac{r_{in,3D}}{r_{circ,3D}}. \tag{1}$$

For a regular tetrahedron, this ratio equals $1/3$, corresponding to a maximum quality index of 1. Fig. 11 shows the mesh quality map of the tetrahedra used to discretize the Fiat 500 model. To overcome the problem, alternative formulations, based on the surface mesh must be considered, where the penetration depth is accounted analytically or semi-analytically.

The surface mesh is generated from the volume mesh by extracting and reassembling the triangular faces lying on the external boundary. For the Fiat 500 model, this procedure resulted in a surface mesh composed of 33,206 triangles, which accurately reproduces the geometry of the original CAD model.

For a 2D mesh, the quality index is defined as the ratio of the radius $r_{in,2D}$ of the inscribed circle and the radius $r_{circ,2D}$ of the circumscribed circle for each triangle:

$$q_{2D} = 2\frac{r_{in,2D}}{r_{circ,2D}}. \tag{2}$$

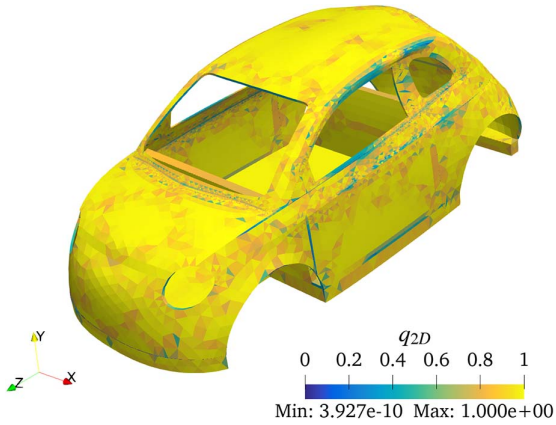


Fig. 12. Map of the 2d mesh quality for the Fiat 500 model.

The 2D mesh quality is mapped in Fig. 12. The quality of the 3D and 2D meshes is quantitatively compared in Fig. 13. Notwithstanding an overall good quality of the meshes, the 3D mesh presents about 1,500 elements with a quality index lower than 0.1. On the contrary, the 2D mesh has an overall better quality, with a median value of 0.9 and only a few outlier elements have a quality factor lower than 0.35, making this mesh suitable for electromagnetic simulations.

In the following analysis, a hybrid formulation using the BEM equation in the air and magnetic non-conductive structures and the SIBC in the conductive region is used [31].

A dynamic WPT system, with 50 transmitting pads (each 1.5 m × 0.5 m), spaced by 0.5 m, is considered. The rear-mounted receiver follows the SAE J2954 standard [3], operating at 85 kHz and 7.7 kW. The excitation currents are set equal to the corresponding values derived in Sec. III-A, i.e. 26 A and j26 A. According to the literature, dynamic WPT systems can be analyzed as stationary ones, with the worst-case exposure occurring during vehicle movement between transmitters [18], [32] as in the case shown in Figs. 14 and 15(a). Due to the rear position of the receiver, the stray magnetic field generated by the transmitter is maximum due to minimal car body shielding.

The human model used is Duke, a 34-year-old male from the virtual population [33]. Tissue dielectric properties are sourced from the IT'IS database [34], except for the skin, whose conductivity is assumed to be 0.1 S/m to limit unrealistically sharp localized peaks of the induced electric field [35], [36], [37], [38]. A resolution of 2 mm × 2 mm × 2 mm is employed. In Fig. 15(a), the human body is 1.3 m from the transmitter center and 0.45 m from the car body. A 3D contour plot highlights regions exceeding 27 μT [39], i.e., the ICNIRP 2010 reference level for public exposure at 85 kHz. It also reports 15 μT, i.e., the limit for people with cardiac implantable electronic devices proposed by SAE J2954 [3], and 6.25 μT, i.e., the ICNIRP 1998 reference level for public exposure [40]. It is apparent that part of the legs of the human model lies within the 6.25 μT region.

Under the considered quasi-static conditions, the perturbation of the source magnetic field due to the human model is negligible; therefore, the field is computed without the body and subsequently used for dosimetry [35]. Induced quantities are calculated using the scalar potential finite difference (SPFD)

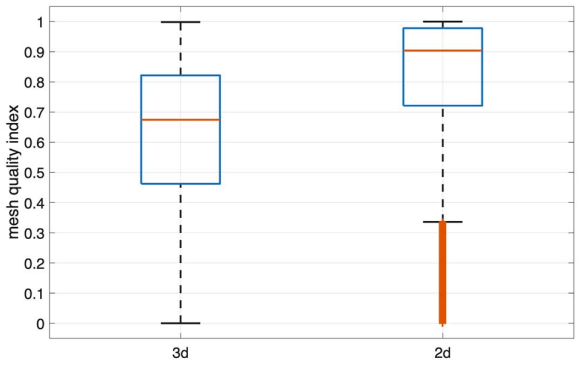


Fig. 13. Boxplot of the 3D and 2D mesh quality indices.

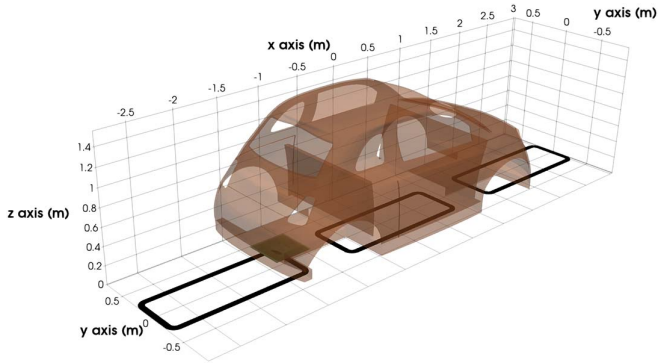


Fig. 14. Dynamic WPT system.

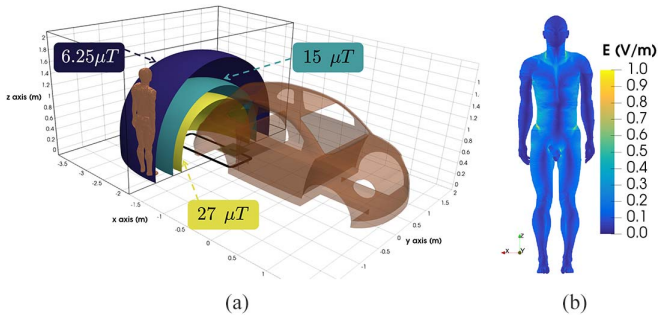


Fig. 15. Magnetic flux density distribution in the worst case (a). induced electric field in the human body (b).

method, with source terms derived from magnetic flux density values in a bounded volume including the human body [31], [41]. The regulatory frameworks define the dosimetric quantities to be computed: the 1998 ICNIRP guidelines require current density averaged over 1 cm^2 [40], while the 2010 guidelines require the 99th percentile of the induced electric field [39]. Moreover, recent advances in numerical dosimetry point out that, for non-uniform exposures, the 99.9th percentile should be preferred to avoid underestimation [42], [43]. Fig. 15(b) shows the induced electric field, and Table II provides 99th and 99.9th percentile values for key tissues. The maximum 1.14 V/m is well below the 11.5 V/m basic restriction (ICNIRP 2010 guidelines). This is expected because the magnetic field exposure remains under 27 μT. However, the maximum induced current density of 169 A/m^2 approaches the 170 A/m^2 basic restriction

TABLE II
INDUCED ELECTRIC FIELD IN TARGET TISSUES

E_{field} (V/m)	Grey matter	White matter	Subcutaneous FAT	FAT	Skin	Spinal cord
E_{99th}	0.11	0.09	0.64	0.49	0.48	0.07
$E_{99.9th}$	0.15	0.11	1.14	0.86	1.05	0.09

(ICNIRP 1998 guidelines), indicating a compliance distance of 0.45 m for the simulated configuration and operating conditions. Closer proximity might be allowed under ICNIRP 2010 guidelines but poses other risks (e.g., collision with the car).

V. CONCLUSION

This work presents Vehicle4em, a four-vehicle CAD database tailored to numerical electromagnetic simulations, designed to support robust meshing and reliable field predictions for problems involving realistic vehicle geometries. These models address practical issues that often make "as-designed" mechanical CAD assemblies difficult to use directly in EM solvers, while retaining the geometric features that govern shielding and eddy-current driven field shaping in the near zone.

Using an SAE J2954-like WPT configuration as a representative low-frequency scenario, the results highlight that oversimplified chassis representations can lead to substantial, spatially dependent errors in stray-field estimates (including localized over/underestimations and, in some regions, deviations on the order of a factor of two), supporting the need for full-vehicle geometry in predictive assessments. Furthermore, comparisons across the shared vehicles show that vehicle geometry diversity has a measurable impact on the predicted field, with peak values along the defined inspection lines differing by roughly a factor of two between models in the presented examples. The final case study demonstrates how the database can be used end-to-end for compliance-oriented workflows that include numerical dosimetry.

Overall, the database (available via [23]) can serve as a reproducible benchmark for future studies on WPT stray-field mitigation, EMC, and human exposure in automotive contexts, and more broadly for EM interactions involving realistic vehicle bodies.

REFERENCES

[1] O. C. Onar, M. Chinthavali, S. L. Campbell, L. E. Seiber, and C. P. White, "Vehicular integration of wireless power transfer systems and hardware interoperability case studies," *IEEE Trans. Ind. Appl.*, vol. 55, no. 5, pp. 5223–5234, Sep. 2019.

[2] V. Cirimele, M. Diana, F. Freschi, and M. Mitolo, "Inductive power transfer for automotive applications: State-of-the-art and future trends," *IEEE Trans. Ind Appl.*, vol. 54, no. 5, pp. 4069–4079, Sep. 2018.

[3] "Wireless power transfer for light-duty plug-in/electric vehicles and alignment methodology J2954_202408," [Online]. Available: https://www.sae.org/standards/content/j2954_202408/

[4] J. Schneider et al., "Validation of wireless power transfer up to 11kW based on SAE J2954 with bench and vehicle testing," in *SAE Technical Paper Series, Ser. ANNUAL*. SAE Int., Apr., 2019.

[5] J. González-González, A. Triviño-Cabrera, and J. Aguado, "Design and validation of a control algorithm for a SAE J2954-compliant wireless charger to guarantee the operational electrical constraints," *Energies*, vol. 11, no. 3, p. 604, Mar. 2018.

[6] "IEC 61980-1:2020 electric vehicle wireless power transfer(WPT) systems—Part 1: General requirements," 2020. [Online]. Available: https://webstore.iec.ch/publication/31657
[7] "Electric vehicle wireless power transfer (WPT) systems - Part 3: Specific requirements for the magnetic field wireless power transfer systems," 2020. [Online]. Available: https://webstore.iec.ch/publication/27435
[8] M. Maemura and A. Wendt, "Dynamic power transfer as a feature - employing stationary WPT devices for dynamic operation," in *Proc. IEEE PELS Workshop Emerg. Technol. Wireless Power Transfer (WoW)*, Piscataway, NJ, USA: IEEE Press, Nov. 2020, pp. 50–55.
[9] B. Vaidya and H. T. Mouftah, "Dynamic wireless charging for CAEV taxi fleet in urban environment," *Internet Technol. Lett.*, vol. 3, no. 6, pp. 1–6, Mar. 2020, doi: 10.1002/itl2.153.
[10] A. Mohamed, P. Schrafel, A. Meintz, and A. Calabro, "Human exposure analysis to EMFs from ground assembly of a WPT system during the vehicle's non-attendance," No. NREL/CP-5400-71887. Nat. Renewable Energy Lab. (NREL), Golden, CO, United States, 2018.
[11] L. Lin, J. Nadakuduti, and P. Guckian, "Compliance assessment of human exposure from wireless electric vehicle charging system using at least one phantom model," U.S. Patent No. 9,575,108, Feb. 2017.
[12] T. Campi, S. Cruciani, F. Maradei, and M. Feliziani, "Magnetic field during wireless charging in an electric vehicle according to standard SAE J2954," *Energies*, vol. 12, no. 9, p. 1795, May 2019.
[13] K. Miwa, T. Takenaka, and A. Hirata, "Electromagnetic dosimetry and compliance for wireless power transfer systems in vehicles," *IEEE Trans. Electromagn. Compat.*, vol. 61, no. 6, pp. 2024–2030, Dec. 2019.
[14] I. Laakso, T. Shimamoto, A. Hirata, and M. Feliziani, "Quasistatic approximation for exposure assessment of wireless power transfer," *IEICE Trans. Commun.*, vol. E98.B, no. 7, pp. 1156–1163, 2015.
[15] S. Park, "Evaluation of electromagnetic exposure during 85 kHz wireless power transfer for electric vehicles," *IEEE Trans. Magn.*, vol. 54, no. 1, pp. 1–8, Jan. 2018.
[16] P.-P. Ding, L. Bernard, L. Pichon, and A. Razek, "Evaluation of electromagnetic fields in human body exposed to wireless inductive charging system," *IEEE Trans. Magn.*, vol. 50, no. 2, pp. 1037–1040, Feb. 2014.
[17] I. Liorni et al., "Assessment of exposure to electric vehicle inductive power transfer systems: Experimental measurements and numerical dosimetry," *Sustainability*, vol. 12, no. 11, p. 4573, Jun. 2020.
[18] V. Cirimele, F. Freschi, L. Giaccone, L. Pichon, and M. Repetto, "Human exposure assessment in dynamic inductive power transfer for automotive applications," *IEEE Trans. Magn.*, vol. 53, no. 6, pp. 1–4, Jun. 2017.
[19] E. Yavolovskaya et al., "Low frequency human exposure analysis for automotive applications," in *Proc. Int. Symp. Electromagn. Compat. - EMC EUROPE*, 2017, pp. 1–6. [Online]. Available: https://api.semanticscholar.org/CorpusID:33589437
[20] F. Freschi, L. Giaccone, V. Cirimele, and L. Solimene, "Vehicle4em: A collection of car models for electromagnetic simulation," in *Proc. IEEE Wireless Power Technol. Conf. Expo (WPTCE)*. Piscataway, NJ, USA: IEEE Press, 2025, pp. 1–6.
[21] V. De Santis, L. Giaccone, and F. Freschi, "Influence of posture and coil position on the safety of a WPT system while recharging a compact EV," *Energies*, vol. 14, no. 21, p. 7248, Nov. 2021.
[22] V. De Santis, L. Giaccone, and F. Freschi, "Chassis influence on the exposure assessment of a compact EV during WPT recharging operations," *Magnetochemistry*, vol. 7, no. 2, p. 25, Feb. 2021.
[23] "vehicle4em - CAD models of vehicles for electromagnetic applications," 2021. Accessed: Mar. 9, 2026. [Online]. Available: https://github.com/cadema-PoliTO/vehicle4em
[24] D. Saha and I. M. Nawi, "Design and data-efficient optimization of a dual-band microstrip planar Yagi antenna for sub-6 GHZ 5G and cellular vehicle-to-everything communication," *Electronics*, vol. 15, no. 1, pp. 1–27, 2026. [Online]. Available: https://www.mdpi.com/2079-9292/15/1/23
[25] W. Schroeder, K. Martin, and B. Lorensen, *The Visualization Toolkit* (4th ed.). Kitware, 2006. pDF version available under CC BY 4.0. [Online]. Available: https://gitlab.kitware.com/vtk/textbook/raw/master/VTKBook/VTKTextBook.pdf
[26] Kitware Inc., "The visualization toolkit (VTK)," https://vtk.org includes downloadable *VTK Textbook* (4th ed.) PDF under CC BY 4.0.
[27] Sandia National Laboratories and Kitware Inc. and Los Alamos National Laboratory, "ParaView: Parallel visualization application," [Online]. Available: https://www.paraview.org/, 2024. version 5.13 released on 2024-08-22.
[28] "meshio - I/O for mesh files," Accessed: Mar. 9, 2026. [Online]. Available: https://github.com/nschloe/meshio
[29] D. Bavastro, A. Canova, F. Freschi, L. Giaccone, and M. Manca, "Magnetic field mitigation at power frequency: Design principles and case studies," *IEEE Trans. Ind Appl.*, vol. 51, no. 3, pp. 2009–2016, May/Jun. 2015.
[30] 16ENG08 EMPIR MICEV Consortium, "Best practice guide for the assessment of EMF exposure from vehicle wireless power transfer systems," Accessed: Mar. 9, 2026. 2021. [Online]. Available: www.micev.eu/
[31] F. Freschi, L. Giaccone, and M. Repetto, "Algebraic formulation of nonlinear surface impedance boundary condition coupled with BEM for unstructured meshes," *Eng. Anal. Boundary Elem.*, vol. 88, pp. 104–114, Mar. 2018.
[32] G. Di Capua et al., "Analysis of dynamic wireless power transfer systems based on behavioral modeling of mutual inductance," *Sustainability*, vol. 13, no. 5, p. 2556, Feb. 2021.
[33] A. Christ et al., "The virtual family–development of surface-based anatomical models of two adults and two children for dosimetric simulations," *Phys. Med. Biol.*, vol. 55, no. 2, pp. N23–N38, Dec. 2009.
[34] C. Baumgartner et al., "IT'IS database for thermal and electromagnetic parameters of biological tissues," Version 4.2, Apr. 2024.
[35] P. Dimbylow, "Development of the female voxel phantom, NAOMI and its application to calculations of induced current densities and electric fields from applied low frequency magnetic and electric fields," *Phys. Med. Biol.*, vol. 50, no. 6, pp. 1047–1070, Feb. 2005.
[36] A. Hirata et al., "Intercomparison of induced fields in Japanese male model for elf magnetic field exposures: Effect of different computational methods and codes," *Radiat. Prot. Dosim.*, vol. 138, no. 3, pp. 237–244, Nov. 2009.
[37] A. Hirata, Y. Takano, Y. Kamimura, and O. Fujiwara, "Effect of the averaging volume and algorithm on the in situ electric field for uniform electric- and magnetic-field exposures," *Phys. Med. Biol.*, vol. 55, no. 9, pp. N243–N252, Apr. 2010.
[38] G. Schmid, S. Cecil, and R. Überbacher, "The role of skin conductivity in a low frequency exposure assessment for peripheral nerve tissue according to the ICNIRP 2010 guidelines," *Phys. Med. Biol.*, vol. 58, no. 13, pp. 4703–4716, Jun. 2013.
[39] ICNIRP, "Guidelines for limiting exposure to time-varying electric and magnetic fields (1 Hz To 100 kHz)," *Health Phys.*, vol. 99, no. 6, pp. 818–836, Dec. 2010.
[40] ICNIRP, "Guidelines for limiting exposure to time-varying electric, magnetic, and electromagnetic fields (up to 300 GHz). international commission on non-ionizing radiation protection," *Health Phys.*, vol. 74, pp. 494–522, Apr. 1998.
[41] I. Laakso, V. De Santis, S. Cruciani, T. Campi, and M. Feliziani, "Modelling of induced electric fields based on incompletely known magnetic fields," *Phys. Med. Biol.*, vol. 62, no. 16, pp. 6567–6578, Jul. 2017.
[42] A. Hirata et al., "Assessment of human exposure to electromagnetic fields: Review and future directions," *IEEE Trans. Electromagn. Compat.*, vol. 63, no. 5, pp. 1619–1630, Oct. 2021.
[43] Y. Diao et al., "Recent advances and future perspective in computational bioelectromagnetics for exposure assessments," *Bioelectromagnetics*, vol. 46, no. 3, pp. 1–24, Feb. 2025, doi: 10.1002/bem.70002.



Fabio Freschi (Senior Member, IEEE) received the M.Sc. (*summa cum laude*) and Ph.D. degrees in electrical engineering from the Politecnico di Torino, Turin, Italy, in 2002 and 2006, respectively. In 2006, he was a Visiting Researcher with the Technical University of Graz, Graz, Austria. He was an Adjunct Senior Fellow with The University of Queensland, Australia, from 2014 to 2020. He is currently a Full Professor in fundamentals of electrical engineering with the Politecnico di Torino and an Honorary Professor, The University of Queensland, Brisbane, QLD, Australia. He co-authored more than 150 conference and journal papers in these fields. His research and scientific interests include numerical modeling and computation of electromagnetic and coupled fields using differential, integral, and hybrid techniques. He is a recipient of several international awards issued by IEEE. In 2022 and 2023, he has been included in the World's 2% Top Scientist list prepared by Stanford University and Elsevier. He was an Associate Editor for IEEE IAS and serves as a Referee of many international journals in the field of numerical electromagnetics, optimization, and operational research.



Luca Giaccone (Senior Member, IEEE) was born in Cuneo, Italy, in 1980. He received the Laurea and Ph.D. degrees in electrical engineering from the Politecnico di Torino, Turin, Italy, in 2005 and 2010, respectively. He works on several areas of the electrical engineering: optimization; modeling of complex energy systems; computation of electromagnetic and thermal fields; energy scavenging; magnetic field mitigation; EMF dosimetry; and compliance of LF pulsed magnetic field sources. Since 2017, he has been an Associate Professor with the Dipartimento Energia "G: Ferraris," Politecnico di Torino. Since 2015, he has been a member of the IEEE International Committee on Electromagnetic Safety—Technical Committee 95 - SC6 - dosimetry modeling. Since 2017, he has been a member of the National Italian Committee CEI-106 dealing with human exposure to electromagnetic fields. He was a member of the ICNIRP Scientific Expert Group (SEG), in 2020.



Vincenzo Cirimele (Senior Member, IEEE) received the M.Sc. degree in electrical engineering (*summa cum laude*) from the Politecnico di Torino, Turin, Italy, in 2013, the Ph.D. degree in electronics engineering (Hons.) from the Politecnico di Torino and the Ph.D. degree in electrical engineering from the Universite Paris-Saclay, in 2017. He was an Assistant Professor with the Department of Energy, Politecnico di Torino, from 2017 to 2020. He is an Associate Professor with the Department of Electrical, Electronic, and Information Engineering, Alma Mater Studiorum University of Bologna, Bologna, Italy. From 2020 to 2021, he was a technical responsible for the R&D and Innovation Group of the company Movyon s.p.a. of Autostrade per l'Italia Group, where he supervised projects related to energy sustainability and development of highway electric mobility. His research interests mainly concern technologies for electric mobility, inductive power transmission, electromagnetic modeling and simulation, and power electronics. He acts as a Deputy Editor for *IET Power Electronics* and an Associate Editor for the journals IEEE TRANSACTIONS ON TRANSPORTATION ELECTRIFICATION and *Wireless Power Transfer*.



Luigi Solimene (Member, IEEE) was born in Avellino, Italy, in 1994. He received the B.S., M.S., and Ph.D. degrees in electrical engineering from the Politecnico di Torino, Turin, Italy, in 2016, 2019, and 2022, respectively. From 2022 to 2023, he was a Research Fellow with the Department of Energy "Galileo Ferraris," Politecnico di Torino, where he is currently an Assistant Professor. His research interests include the design and optimization of magnetic devices for electrical energy conversion, inductive and capacitive wireless power transfer systems, the characterization of soft magnetic materials, and data-driven modeling for electromagnetic devices.

Open Access funding provided by 'Politecnico di Torino 2025-2027 Deposit Account' within the CRUI CARE Agreement